Electronic Journal of Structural Engineering

Original Article

Cite this: DOI:10.56748/ejse.25714

Received Date: 25 November 2025
Accepted Date: 19 March 2025

1443-9255
https://ejsei.com/ejse

Stability analysis of surrounding rocks of deeply buried underground chambers based on the improved block theory and simulation using unwedge computer program

Fugui Tao [a*], Anyi Lan [b], Lei Han [a], Xudan Sun [c], Zhixi Liu [d]

[a] Associate Professor, Zhangjiakou Vocational and Technical College, Zhangjiakou, 075031, China.
[b] Associate Professor, Hebei North University, Zhangjiakou, 075132, China
[c] Lecturer, PhD, Zhangjiakou Vocational and Technical College, Zhangjiakou, 075031, China.
[d] Associate Professor, Ph.D., Beijing University of Science and Technology, Beijing, 100083, China.
*Corresponding author: tfugui88@163.com

Abstract

To tackle the challenges of extensive drawing workloads and limited precision inherent in the application of block theory, this paper presents an optimization of block theory based on an improved vector method. Additionally, the Unwedge computer program is employed to conduct visual simulations of block theory applications, thereby enhancing the ease of utilizing block theory. To validate the accuracy of our research findings, we conducted a case study on the stability of surrounding rock in deeply buried underground caverns with complex geological structures at Jinping-II Hydropower Station. The research results reveal that the refined vector method can swiftly identify the stability of surrounding rock in various study areas, offering a valuable reference for the practical excavation of underground caverns. In the engineering case, safety concerns arise in key block zones with safety factors below 1.5, necessitating the implementation of appropriate safety measures during excavation. Furthermore, some key blocks exhibit a safety factor of zero and are positioned at the top of the cavern. In theory, these key blocks could have a certain impact on the stability of the surrounding rock of the cavern. However, given their small volume and weight, they can be deemed stable. By comparing the refined block theory and computer program calculation results with the actual construction and excavation process of the underground cavern, we found that they are largely consistent. This underscores that the improved method proposed in this paper can provide theoretical support and a feasible basis for the excavation of deeply buried underground caverns.

Keywords

Improved block theory, Unwedge program, Computer simulation, Underground chambers, Surrounding rock stability

1. Introduction

Deeply buried chambers are constructed under complex geological conditions and are greatly affected by natural geological states (geostress, geological physical parameters, groundwater, and faults) and artificial excavation (excavation patterns, support patterns, and timing). Due to the large burial depth, added with complex geological structures, underground chambers are in an extremely complex geological environment, for which stability analysis of surrounding rocks is very difficult. With the flourishing of large-scale underground engineering in each country, underground chambers are increasingly up scaled, and their burial depth becomes increasingly large, which also sets higher requirements for stability. In the meantime, due to the complexity and unpredictability of various geological conditions that influence the stability of chambers, the stability analysis of surrounding rocks of underground chambers has become the major issue of underground engineering. It is not only related to whether hydropower stations can be smoothly constructed and commissioned or not, but also, to a large extent, determines the investment and construction period of engineering. Although rich experience has been accumulated through numerous underground engineering practices. Even though the basic geological conditions and engineering characteristics of surrounding rocks of chambers are not well understood because engineering geological survey is not detailed and deep enough, and stability analysis and evaluation methods are less reasonable. As a result, some chambers suffer large-scale collapse during construction, so that construction cannot proceed, and the chambers are even abandoned. Some chambers experience deformation and failure during operation, which seriously influences their use. Considering this, it is necessary to take complex engineering measures.

The block theory has gradually developed and improved since the mid-1980s. In the efforts of American professor R.E. Goodman and Chinese professor Shi, the block theory has gradually developed into an important theory for stability analysis of rock engineering (Wang et al. 2020; Zhang et al. 2023). The block theory is a stability analysis method of block rock mass by virtue of the topology, set theory, geometry, and vector algebra and has been widely used in the world. The block theory is mainly applied under the following assumptions: 1) structural planes in the rock mass are all planes and run through the whole rock mass; 2) structural bodies are all rigid bodies; 3) failure mode of rock mass under various loads is firstly shown as shear displacement along structural planes. On the basis of the above assumptions, structural planes and free excavation faces are regarded as spatial planes at first. That is to say, structural bodies are considered as asperities and various loads as spatial vectors, thus using geometric methods for mobility and stability analysis of blocks under spatial plane conditions (Mahdevari et al. 2020; Loss. 2021).

The block theory is highly reliable in theoretical computation of deeply buried underground chambers. To facilitate the utilization of the theory, researchers have developed Unwedge programs on the basis of block theory. This program is primarily used to analyze the stability of blocks formed in hard rock masses. It features a user-friendly interface, supports interactive operation, and can intuitively display spatial geometric shapes. The program can also be utilized for analysis and computation of anchor reinforcement of unstable blocks (Fu et al. 2021; Qiang and Li 2021; Lodge et al. 2022). It is able to automatically generate and search for the largest possible wedged blocks and calculate their safety factors. According to the calculation results of the program, users can screen and further analyze the formed blocks combining with actual outcrop.

However, the application of block theory is often hindered by substantial drawing workloads, limited precision, and challenges related to visualization and usability. To address these issues, this paper introduces an optimization of block theory based on an advanced vector method. Furthermore, the Unwedge computer program is employed to conduct visual simulations of block theory applications, thereby significantly enhancing the convenience of its utilization. To validate the accuracy of our research findings, an in-depth engineering case study was conducted on the underground caverns of the Jinping-II Hydropower Station. The analysis and verification undertaken in this study not only confirmed the feasibility of the research method proposed in this paper but also provided practical and reproducible guidance for actual construction projects.

2. Improved block theory

2.1 Basic types of blocks

Blocks can be classified into two types: finite and infinite blocks. Therein, finite blocks are constituted by movable and immovable blocks; meanwhile, possibly unstable blocks, stable blocks, and key blocks constitute movable blocks, as shown in Fig. 1.

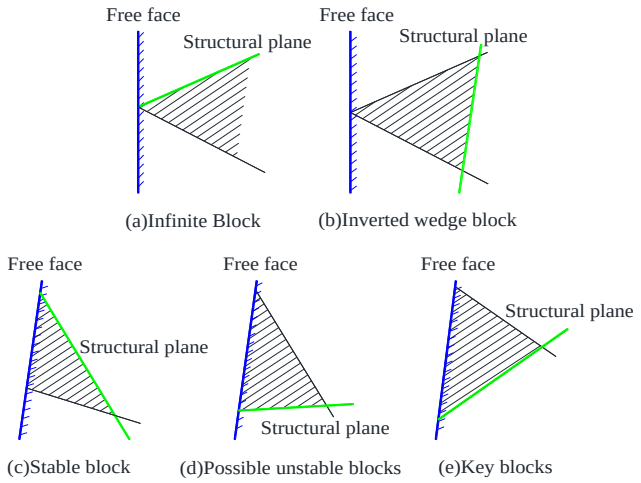

Fig. 1 Block classification

2.2 Types of pyramids

Pyramids are formed by translation of various structural planes and free faces in space, so that the origin is located on each structural plane to form a series of tetrahedrons with the origin of coordinates as the vertex (Zerradi et al. 2020; Sarkar et al. 2021; Abdallah et al. 2023). There are the following several types of pyramids:

(1) Joint pyramid (JP), which is formed by the half-space of rock mass only bounded by structural planes;
(2) Excavation pyramid (EP), which is formed by the half-space of rock mass only bounded by free faces;
(3) Space pyramid (SP), which is the pyramid beyond the EP;
(4) Block pyramid (BP), which is formed by the half-space of rock mass bounded by several structural planes and more than one free face.

In analytic geometry, the equation for structural planes in the rock mass is expressed as follows:

$$Ax + By + Cz = D \tag{1}$$

Geometrically, the space is divided into two half-spaces by a single structural plane. Then, the following expression can be used to represent the half-space:

$$Ax + By + Cz \geq D \tag{2}$$

The equation set of blocks formed by n half-spaces is expressed as

$$\begin{cases} A_1x + B_1y + C_1z \geq D_1 \\ A_2x + B_2y + C_2z \geq D_2 \\ A_3x + B_3y + C_3z \geq D_3 \\ \cdots\cdots \\ A_nx + B_ny + C_nz \geq D_n \end{cases} \tag{3}$$

Generally, an n-faced block can be expressed by n inequations, and the intersection of n half-spaces is the block. Eqns. (1) ~ (3) all contain D that represents the detailed spatial locations of half-spaces, planes, and blocks.

Various planes are translated one by one through the origin. Then, 0 can be used to replace D in the above equations. Pyramids are formed by each plane of blocks that pass through the origin. That is to say, the intersection of half-spaces that pass the origin of coordinates is a pyramid.

2.3 Finite and mobility theories of blocks

Infinite and finite blocks are both formed by cutting structural planes. What is available for engineering are finite blocks. The finite theory of block theory is

$$JPIEP = \Phi, \ \Phi \text{ is null set} \tag{4}$$

If the solution of Eq. (3) is unique and a zero solution, the corresponding blocks are finite ones. Assuming that Eq. (3) has a non-zero solution, that is, there are block pyramids, then the corresponding blocks are infinite blocks.

If one block is a finite block formed by intersection of structural planes and free faces and the fracture block is an infinite block, the block is a movable block; if the formed block and the fracture block are both finite blocks, then the block is an immovable block. It can be expressed by the following equation:

$$JP \neq \Phi \text{ and } JPIEP = \Phi \text{ or } JP \subset SP \tag{5}$$

As a whole, the general method based on block theory is to exclude all immovable and infinite blocks through geometrical analysis. Then, blocks that may become instable under all kinds of loads are analyzed on the basis of kinematics. Finally, key blocks on the excavation face are ascertained based on known physical and mechanical properties of gliding planes (Shrestha. 2020; Haryono and Purwodihardjo 2021; He et al. 2021; Janiszewski et al. 2021).

2.4 Stability evaluation of blocks directly separating from rock mass

Under the condition, blocks are only under the active resultant force ¯r, without resistance. That is, the safety factor can be designed to be 0.

2.5 Stability evaluation of blocks during single face sliding

When using the ultimate equilibrium, the ratio of sliding resistance to sliding force on the griding plane is the safety factor. Considering cohesion, safety factor F can be calculated using the following formula:

$$F_c = \frac{N_i \cdot f_i + C_i \cdot A_i}{T_i} \tag{6}$$

where f_i and C_i separately represent the friction coefficient and cohesion; A_i is the area of griding plane; T_i and N_i are separately the tangential and normal components of $\overline{r}$ on the griding plane i, in which $N_i = |\overline{r} \cdot \overline{n_i}|$ $T_i = |\overline{r} \cdot \overline{n_i}|$. The expression of safety factor (not considering cohesion) is

$$F_0 = \frac{N_i \cdot f_i}{T_i} \tag{7}$$

2.6 Stability evaluation of blocks during double-face sliding

When considering cohesion, the safety factor is expressed as follows:

$$F_c = \frac{N_i \cdot f_i + C_i \cdot A_i + N_j \cdot f_j + C_j \cdot A_j}{T_{ij}} \tag{8}$$

2.7 Improved block theory

In the application of the aforementioned block theory for computational and stability evaluations, a substantial workload related to graphical representation frequently arises. To mitigate this challenge, this paper introduces an optimization of block theory usage through the construction of joint cones, leveraging the vector method. In rock mass engineering scenarios featuring four sets of structural planes, tetrahedra and pentahedra constitute the primary geometric shapes. Tetrahedra are formed through the intersection of three of these structural planes with the excavation surface, whereas pentahedra results from the interaction of all four structural planes with the excavation surface. Assuming the four sets of structural planes are designated as J1, J2, J3, and J4, there emerge five potential combinations: J1-J2-J3-J4, J1-J2-J3, J1-J2-J4, J1-J3-J4, and J2-J3-J4. Hence, in identifying the largest movable block, it is imperative to comprehensively consider the joint cones formed by combinations of both three and four structural planes. This paper adopts the vector method to facilitate the construction of various joint cones, with the normal vectors of the structural planes derived from the average values of their respective parameters:

$$n_i = (sin\alpha_i sin\beta_i, cos\alpha_i sin\beta_i cos\beta_i) \tag{9}$$

The joint cone JP_r is represented as JP ($a_1a_2\ldots a_m$), where r denotes the number of the joint cone, with r ranging from 1 to 2^m; a_i represents the positional parameter of the joint cone; a_i=0 indicates that the joint cone is located above the ith structural plane, while a_i=1 indicates that it is below the ith structural plane. An $m \times m$ diagonal matrix is constructed according to the following formula:

$$G_{JP(a_1a_2\ldots a_m)} = \mathrm{diag}(-2a_1 + 1, -2a_2 + 1, \ldots, -2a_m + 1) \tag{10}$$

When constructing a joint cone using three structural planes, there are three intersection lines between the planes, and their direction vectors can be represented as N:

$$N = (n_1 \times n_2, n_1 \times n_3, n_2 \times n_3)^{\mathrm{T}} \tag{11}$$

The expression for the edge vector set of the joint cone JP_r can then be obtained as:

$$V_r = E_r N \tag{12}$$

In practical applications, the Y-axis represents the tunnel strike, and the Z-axis points vertically upwards. When forming the largest block, the excavation surface is tangent to the edge ridge line of JP. The vertex of the largest block is the intersection of four ridge lines, which are also the intersections of four structural planes. When the excavation surface is represented by a single curve, it is easy to determine the ridge line location through the tangency condition. However, when the excavation surface is composed of multiple curves, one must first determine which edge ridge line is tangent to before locating it. At this point, the ridge line of the joint cone is projected onto the XOZ plane, and the edge ridge line of the joint cone can be determined by the maximum included angle. Based on this, the stability coefficient of the block can be quickly obtained.

3. Visual simulation using the unwedge computer program

After calculating the stability coefficient of the surrounding rock in a deeply buried underground cavern using the improved block theory, further visual simulation is conducted through the Unwedge computer program. The simulation results are then compared and validated with theoretical calculations and actual excavation data to guide the construction process on site.

3.1 Basic principles

Stress on the blocks can be classified into two types: active force and passive force. When calculating the theoretical safety factor using the program, the active force is the sliding force, while the sliding resistance is the passive force (Hustrulid and Johnson 2020; Paraskevopoulou and Boutsis 2020; Khodr et al. 2023; Lemos et al. 2024).

3.2 Active vectors

Active vectors can be calculated using Eq. (13).

$$A = W + C + X + U + E \tag{13}$$

where A is the vector of active force; W is the gravitational vector of blocks; C is the gravitational vector of shotcrete; X is the vector of active pressure; U is the vector of water pressure; E is the seismic vector.

(1) Gravitational vector

The gravitational vector is the main sliding force, which is calculated using the following formula:

$$W = (\gamma_r \cdot v) \cdot \vec{g} \tag{14}$$

where W is the gravitational vector; γ_r is the unit weight of blocks; v is the volume; $\vec{g}$ is the direction vector of gravity.

(2) Gravitational vector of concrete

In general cases, this part of gravitational vector is negligible, while it needs to be considered if the concrete reaches a certain thickness. The calculation formula is

$$C = (\gamma_s \cdot t \cdot a_e) \cdot \vec{g} \tag{15}$$

where C is the gravitational vector of concrete; γ_s is the unit weight of concrete; t is the thickness of concrete; a_e is the projection of blocks on the free face; $\vec{g}$ is the direction vector of gravity.

(3) Vector of active pressure

In the program, the vector of active pressure can be expressed using the following calculation formula:

$$X = \sum_{i=1}^{3} p_i a_i \vec{n_i} \tag{16}$$

where p_i is the pressure on block face i; $\vec{n_i}$ is the normal vector on face i; X is the vector of active pressure; a_i is the area of face i.

(4) Vector of water pressure

Hydrostatic and hydrodynamic pressures are parameters needed in computational analysis of each structural plane in the program.

1) Hydrostatic pressure

$$U = \sum_{i=1}^{3} u_i a_i \vec{n_i} \tag{17}$$

where a_i is the area of face i; U is the vector of hydrostatic pressure; u_i is the water pressure on structural plane i; $\vec{n_i}$ is the normal vector on face i.

2) Hydrodynamic pressure

The hydrodynamic pressure is assumed to change linearly with the depth in Unwedge program, so triangulation is performed for each face in the computation. After calculating the water pressure on each triangular element, the sum of water pressures on various triangular elements is the water pressure on each structural plane. The calculation formula is

$$U = \sum_{i=1}^{3} \sum_{j=1}^{n} r_w h_{ij} a_{ij} \vec{n_i} \tag{18}$$

where U is the vector of hydrodynamic pressure; i is the structural plane of a block beyond the outcrop of the free face; j is a triangular element on face i; n is the number of triangular elements triangulated on face i; a_{ij} is the area of triangular element j on face i; $\vec{n_i}$ is the normal vector in the direction i; h_{ij} is the average depth of triangular element j below the surface, in which $h_{ij} = 1/3 \sum_{i=1}^{3}(gse - y_i)$; gse is the surface elevation; y_i is the elevation of vertexes of triangular elements on face i.

(5) Seismic vector

In Unwedge program, the seismic vector can be calculated using the following formula after determining seismic coefficients in each direction.

$$E = (k \cdot \gamma_r \cdot V) \cdot \vec{e} \tag{19}$$

where k is the seismic coefficient; E is the seismic vector; V is the block volume; γ_r is the unit weight of rocks; $\vec{e}$ is the direction vector of seismic force.

3.3 Vectors of passive forces

The anchoring force of bolts, supporting force of concrete, and passive pressure constitute main passive forces of the system. Vectors of passive forces can be expressed by Eq. (20):

$$P = H + Y + B \tag{20}$$

where H is the vector of shearing resistance of concrete; P is the vector of passive force; B is the vector of anchoring force of bolts; Y is the vector of passive pressure.

(1) Vector of passive pressure

$$Y = \sum_{i=1}^{3} p_i \cdot a_i \cdot \vec{n_i} \tag{21}$$

where p_i is the pressure on face i of blocks; Y is the vector of passive pressure; a_i is the area of face i; $\vec{n_i}$ is the outgoing normal vector on face i.

(2) Vector of shearing resistance of concrete

The vector of shearing resistance of concrete mainly plays a partial support role, and concrete directly infiltrates in the boundary surface to play a reinforcement role.

(3) Vector of anchoring force

The vector mainly plays a role in support via the tensile and shear capacities. Generally, the safety factor is designed in the range of 1.25 ~ 2.0 under different geological conditions. When using the shear mode in the design,

$$N = \frac{T}{f_{sv} A_s} = \frac{K_s \cdot F_X - F_k}{f_{sv} A_s} \tag{22}$$

The following is generally used in tensile design

$$N = \frac{K_s G_f}{T} \tag{23}$$

where K_s is the designed safety factor; T is the anchoring force needed for blocks; F_x is the resistance of blocks; A_s is the area of anchor bolts; f_{sv} is the shear strength of anchor bolts; T is the designed tensile capacity of a single anchor bolt; G_f is the remaining sliding force of unstable blocks; N is the number of anchor bolts needed. The maximum values of Eqns. (22) and (23) are taken in the design.

3.4 Analysis of safety factors

Three safety factors are mainly used in the computation of the program, namely, safety factors without support, safety factors during sliding, and safety factor with support (Hosseini. 2016; Potvin et al. 2019; Lenjani and Nikjo 2021; Sengani and Mulenga. 2022). The final design result is to take the maximum of the three.

(1) Safety factors during sliding (F_f)

During analysis in the case, only passive pressure and tensile strength are considered. The active force mainly plays a role as the sliding thrust and the sliding direction is the direction of the vector of active force. The calculation formula is

$$F_f = \frac{-p \cdot \vec{s_0} + \sum_{i=1}^{3} T_i}{A \cdot \vec{s_0}} \tag{24}$$

where F_f is the safety factor; P is the vector of passive force; S is the vector of active force; T_i is the resistance contributed by tensile strength on structural plane i; $\vec{s_0}$ is the direction vector during sliding.

(2) Safety factor without support (F_u)

During calculation under the condition, the resistance contributed by shear and tensile strengths serve as the main sliding resistance. The calculation formula is

$$F_u = \frac{\sum_{i=1}^{3} J_i^u + T_i}{A \cdot \vec{s_0}} \tag{25}$$

where A sit the vector of active force; F_u is the safety factor without support; T_i is the resistance contributed by tensile strength under condition without support; J_i^u is the resistance contributed by shear strength under condition without support; $\vec{s_0}$ is the vector in the slip direction of blocks.

(3) Safety factor with support (F_s)

When calculating this safety factor, the resistances contributed by passive support, shear strength, and tensile strength all need to be considered. In addition, the resultant force of active and passive forces generates the following normal force:

$$F_s = \frac{-P \cdot \vec{s} + \sum_{i=1}^{3} (J_i^s + T_i)}{A \cdot \vec{s}} \tag{26}$$

where P is the vector of passive force; $\vec{s}$ is the vector in the slip direction of blocks; F_s is the safety factor with support; J_i^s is the resistance contributed by shear strength under condition with support; A is the vector of active force; T_i is the resistance contributed by tensile strength under condition with support.

4. Engineering application

4.1 Engineering Overview

Jinping Ⅱ Hydropower Station is located at Jinping bend along the trunk stream of Yalong River at the junction of three counties, namely, Muli Tibetan Autonomous County, Yanyuan County, and Mianning County (Liangshan Yi Autonomous Prefecture, Sichuan Province, China). Yalong River, as the largest tributary of Jinsha River, springs from the southern foothill of Bayan Har Mountains in Yushu County (Qinghai Province, China). Yalong River runs from northwest to southeast and turns northeastward at Wali village after passing by Yajiang County, then circling Jinping Mountain to form a large river bend 150 km to Bazhe village. It runs southward after passing by Bazhe and finally flows to Jinsha River at Luoguo village downstream of Panzhihua City. The truck stream

of Yalong River has a total length of 1,570 km and the drainage area covers 136,000 km2. The excavated area of underground chambers is shown on Fig. 2.

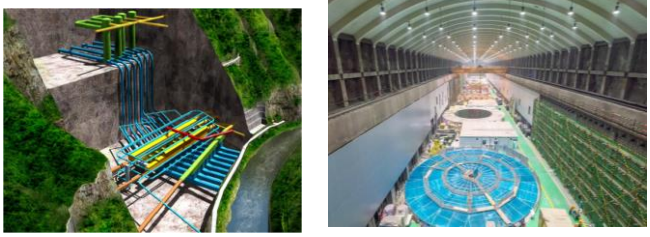

(a) Rendering of the hydropower station hub

(b) Current excavation and construction area

Fig. 2 Excavated area of underground chambers

4.2 Geological Overview

Based on the block theory, the research region belongs to Sichuan-Yunnan lozenge-shaped block. Regional formations can be divided into Kangdian zone (Ⅰ), Yanyuan-Lijiang zone (Ⅱ), and Barkam zone (Ⅲ). The outcropped formations mainly include the lower Ordovician series and lower Silurian series of lower Paleozoic; middle-upper Carboniferous series and Permian system of upper Paleozoic; and Mesozoic Triassic system. The lower Paleozoic is a set of ultrathick clastic rocks experiencing middle and low regional metamorphism; upper Paleozoic and Mesozoic mainly include regional metamorphic carbonatite, clastic rocks and basalt, and pyroclastic rocks, which are mainly distributed at the western end of Jinping bend of Yalong River and the interfluvial block of the large river bend. The eastern end of the large river bend mainly has Presinian metamorphic series, Paleozoic carbonatite, Emeishan basalts and clastic rocks, and Mesozoic clastic and clay rocks. Deposits accumulated from the middle Pleistocene are mainly distributed sporadically along river valleys and foothills.

From the perspective of geotectonics, Jinping Ⅱ Hydropower Station is situated in the southeastern part of Songpan-Ganzi geosynclinal folded system, experiencing Indosinian movement, Yanshanian movement, and especially Himalayan movement since Mesozoic. Therefore, a series of imbricated thrust faults, overturned strata, A-shaped recumbent folds and stretching lineations, and klippes formed along faults are developed, forming strongly deformed fold and fault belts at the platform edge. Yajiang fold belt is a geosynclinal fold belt formed from Paleozoic to Triassic. Indosinian movement at the end of Triassic enabled return of folds, and Yanshanian movement influenced the research region, with granite intrusion. The Himalayan movement causes strong uplifts in the region, accompanied by fracturing activities.

4.3 Lithology

Formations outcropped in the research region are middle Triassic Yantang Formation (T_{2y}) and Quaternary system (Q). Formations from old to new are described as follows:

(1) Yantang formation (T_{2y})

T_{2y}^{4}: Gray-green banded mica marble, in which dark minerals commonly exhibit concentrated distribution in strips along beddings, which are distributed alternately with white marble, forming clear green-white or black-white beddings. The thickness reaches 400 m.

$T_{2y}^{5-(1)}$: Gray-black medium-grained crystalline marble with intercalation of white coarse-grained thick marble layer, below which is dark-gray fine-grained marble with intercalation of greyish-white fine stripes, locally with black crystalline limestone or argillaceous limestone.

$T_{2y}^{5-(2)}$: Greyish white to white coarse-grained marble (containing H2S), which is shown as thick blocks, with gray to greyish-white onyx marble, gray to gray-black porphyritic marble, and greyish-white porphyritic marble in local areas. The above two are main formations around the powerhouse and the outcrop is about 400 m thick.

T_{2y}^{6}: Gray to gray-black middle-thin argillaceous limestone, with local intercalation of dark-gray medium-thick tight massive marble. Bedding is developed and surface rocks are easily weathered. The formation is distributed widely and outcropped above 1,870 m on the surface of powerhouse, with a thickness of 350 m.

(2) Quaternary system (Q)

The Quaternary system is mainly distributed on gentle slopes, in gullies, and below steep cliffs and is dominated by residual deposits, slope deposit, and breccia, along with collapsed deposits and alluvial deposits in local areas.

4.4 Visual analysis of surrounding rock stability

Surrounding rocks of the underground powerhouse are mainly class-Ⅲ surrounding rocks, which account for 83.5% of the total length of chambers; some are class-Ⅱ surrounding rocks (14.1%); a few are class-Ⅳ surrounding rocks (2.4%). During stability analysis, the surrounding rocks are divided into the following four zones:

(1) Greyish white to white coarse-grained marble (containing H_2S), which is thick blocks, with gray to greyish-white onyx marble, gray to gray-black porphyritic marble, and greyish-white porphyritic marble ($T_{2y}^{5-(2)}$) in local areas. The zone is labeled as I and was measured with survey line C in field.

(2) Gray-black medium-fine-grained crystalline marble with intercalation of white coarse-grained thick marble layer, below which is dark-gray fine-grained marble with intercalation of greyish-white fine stripes, locally with black crystalline limestone or argillaceous limestone ($T_{2y}^{5-(1)}$). The zone is labeled as II and was measured with survey line B in field.

(3) Gray to gray-black middle-thin argillaceous limestone, with local intercalation of dark-gray medium-thick tight massive marble. Bedding is developed and surface rocks are easily weathered. The formation is distributed widely and outcropped above 1,870 m on the surface of powerhouse, with a thickness of 350 m (T_{2y}^{6}). The zone is labeled as Ⅲ and was measured with survey line D in field.

(4) Gray-green banded mica marble, in which dark minerals commonly exhibit concentrated distribution in strips along beddings and they are distributed alternately with white marble, forming clear green-white or black-white beddings. The thickness reaches 400 m (T_{2y}^{4}). The zone is labeled as Ⅳ and was measured with survey line A in field.

Because three different lithologies are distributed in the research region, Unwedge program was adopted to analyze surrounding rock stability of underground powerhouse in zones Ⅰ ~ Ⅳ.

Stability analysis of surrounding rocks in zone I

As revealed by survey line C, four groups of dominant structural planes are mainly developed in the zone, namely, J_1 (25°, 73°), J_2 (77°, 306°), J_3 (55°, 255°), and J_4 (56°, 234°). The stereographic projections of these groups of structural planes and the modeling of the underground powerhouse and chamber are shown in Fig. 3.

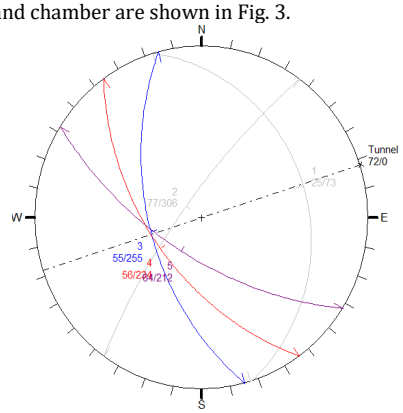

(a) Stereographic projections of structural planes

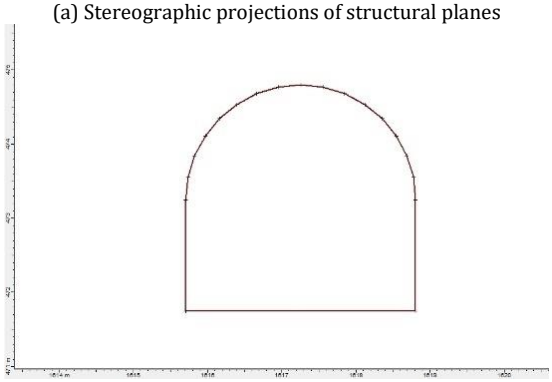

(b) Modeling of the underground chamber

Fig. 3 Stereoscopic projection of structural planes in Section I and modeling of caverns

(1) Setting of basic parameters and parameters of structural planes

With regard to parameter setting, the parameters needing to be input mainly include the axial slope, strike, seismic parameters, and safety factors of tunnels. Parameters of structural planes mainly include cohesion, shear strength, and friction angles. The setting process is mainly displayed in Fig. 4. The calculation parameters for various rock masses and structural planes are shown in Table 1.

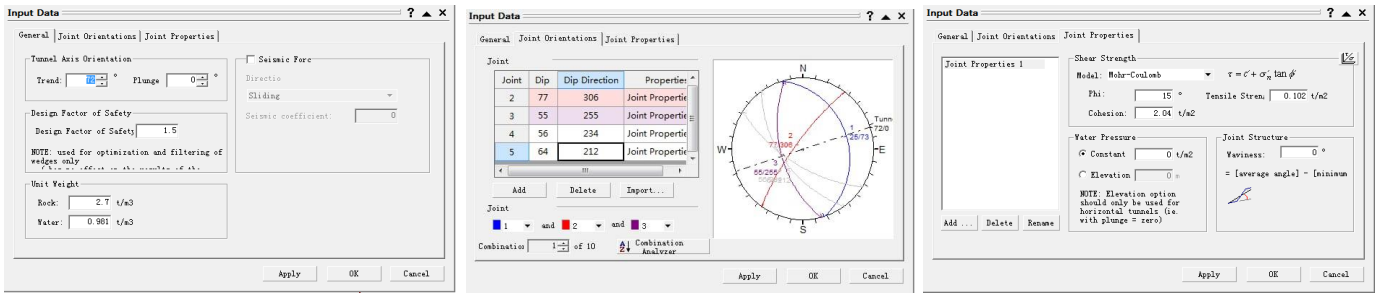

(a) Basic parameters (b) Structural planes (c) Mechanical parameters

Fig. 4 Process of setting parameters for tunnels and structural surfaces

Table 1. Mechanical Parameters of Rock Mass

Surrounding rock classification	Lithology	Wet density /(kN/m³)	Elastic modulus /(10³MPa)		Poisson's ratio	Shear strength	
			Horizontal	Vertical		ϕ/°	c/MPa
II	Striped mica marble (T_{2y}^{4})	28.0	20~25	15~20	0.21	25~40	1.10~1.20
	Medium thick layer marble ($T_{2y}^{5-(1)}$)	27.0	22~35	20~30	0.21		
	Medium thick layer marble ($T_{2y}^{5-(2)}$)	27.1	15~22	15~20	0.22		
	Muddy limestone (T_{2y}^{6})	27.0	16~17	13~15	0.27		
III	Striped mica marble (T_{2y}^{4})	27.0~27.5	9~16	8~15	0.23~0.26	20~30	0.70~1.00
	Medium thick layer marble ($T_{2y}^{5-(1)}$)	26.0~26.5	12~17	9~15	0.23~0.26		
	Medium thick layer marble ($T_{2y}^{5-(2)}$)	26.0~26.6	11~16	7~15	0.25~0.27		
	Muddy limestone (T_{2y}^{6})	26.0~26.5	9~15	6~12	0.28~0.30		
Fault type structural plane	Mud rock debris type structural plane	/	/	/	/	10~20	0.03~0.04
	Rock debris mixed with mud type	/	/	/	/	15~20	0.07~0.08
	Rock fragment type structural plane	/	/	/	/	20~30	0.15~0.20
General structural plane	No filling, closed	/	/	/	/	10	0
	Filling type	/	/	/	/	10	0
	Micro tension type	/	/	/	/	10	0

(2) Generation of key blocks

After inputting structural planes in the program, the program automatically generates all possible maximum key blocks. The key blocks are outcropped at locations shown in Fig. 5. The geometrical characteristics and safety factors of key blocks are listed in Table 2.

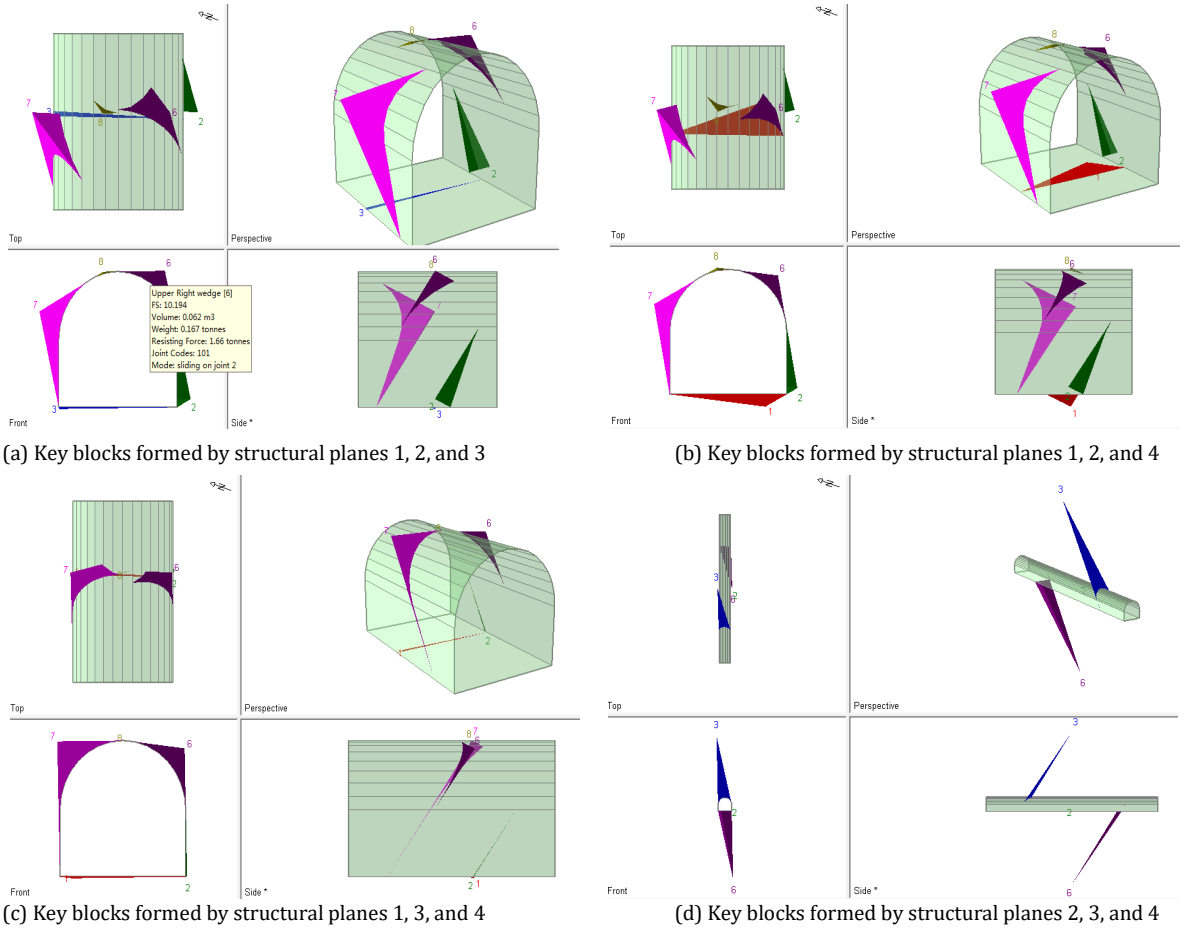

(a) Key blocks formed by structural planes 1, 2, and 3 (b) Key blocks formed by structural planes 1, 2, and 4

(c) Key blocks formed by structural planes 1, 3, and 4 (d) Key blocks formed by structural planes 2, 3, and 4

Fig. 5 Visualization of key block exposure positions in Zone I

Table 2. Geometrical characteristics and safety factors of key blocks in zone I

Structural planes forming key blocks	Key blocks	Locations of key blocks	Safety factors	Block volumes (m^3)	Block weights (t)
1, 2, 3	1	Lower right part of chamber wall	42.627	0.045	0.120
	2	Bottom of chamber	Stable	0.002	0.006
	3	Upper right part of chamber wall	10.194	0.062	0.167
	4	Upper left part of chamber wall	10.909	0.191	0.516
	5	Top of chamber	47.146	0.001	0.001
1, 2, 4	6	Upper left part of chamber wall	9.953	0.170	0.459
	7	Bottom of chamber	Stable	0.133	0.359
	8	Lower right part of chamber wall	39.031	0.035	0.095
	9	Upper right part of chamber wall	9.944	0.050	0.134
	10	Top of chamber	30.964	0.001	0.004
1, 3, 4	11	Lower right part of chamber wall	45.098	0.0001	0.0001
	12	Bottom of chamber	Stable	0.002	0.005
	13	Upper right part of chamber wall	25.805	0.032	0.086
	14	Upper left part of chamber wall	21.799	0.062	0.167
	15	Top of chamber	319.406	0.00001	0.0001
2, 3, 4	16	Bottom of chamber	Stable	7.106	19.187
	17	Upper right part of chamber wall	968.048	0.0001	0.0001
	18	Top of chamber	8.812	5.509	14.873

(3) Stability analysis of key blocks

1) Key blocks 16 and 18 formed by structural planes 2, 3, and 4 are characterized by large volumes and weights, which may pose a certain threat in principle. Key block 16 is considered stable because it is located at the bottom of chamber. The safety factor of key block 18 is 8.812, indicating that the key block is relatively stable, while it is suggested to take certain protective measures during mining due to its location at the top.

2) Aside from the key blocks mentioned above, others key blocks all have large safety factors, while small volumes and weights, so they are all relatively stable. Hence, surrounding rocks in the zone can be regarded stable.

Stability analysis of surrounding rocks in Zone Ⅱ

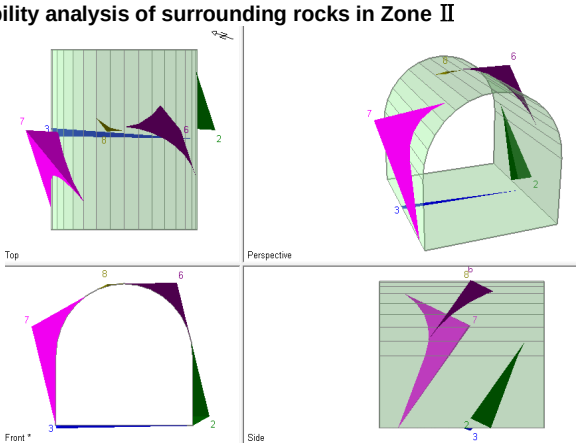

(a) Key blocks formed by structural planes 1, 2, and 3

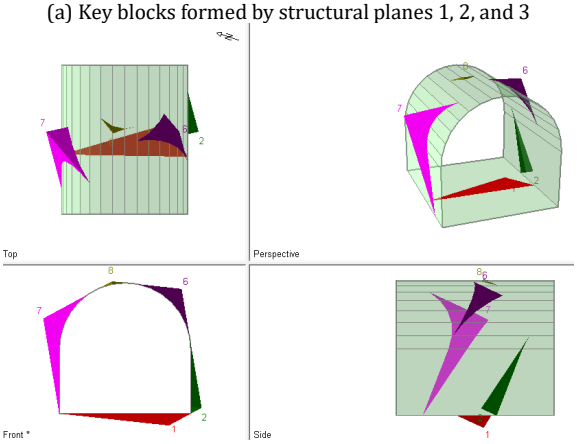

(b) Key blocks formed by structural planes 1, 2, and 4

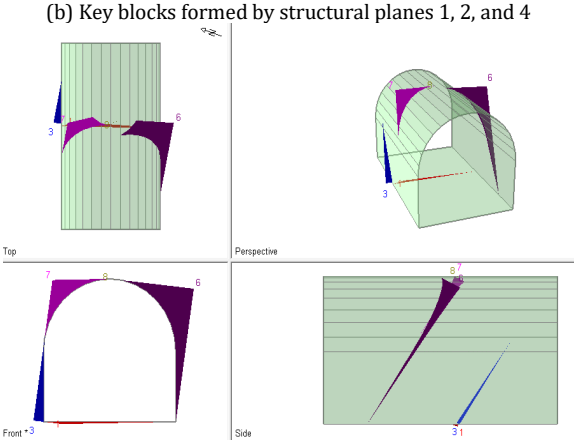

(c) Key blocks formed by structural planes 1, 3, and 4

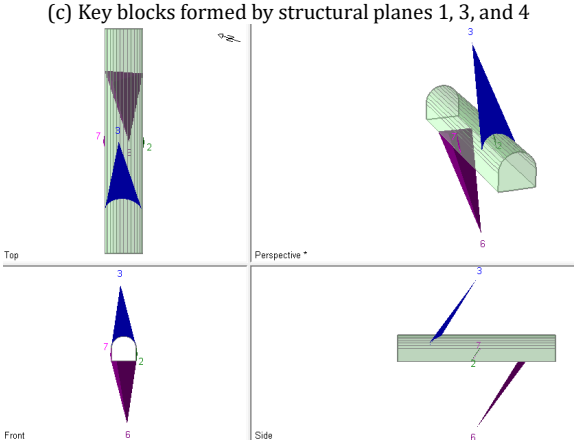

(d) Key blocks formed by structural planes 2, 3, and 4

Fig. 6 Visualization of key block exposure positions in Zone Ⅱ

Data obtained from survey line B reveal that there are mainly four groups of dominated structural planes in the zone, namely, J1 (25°, 73°), J2 (77°, 306°), J3 (54°, 256°), and J4 (57°, 236°). Rock in the zone mainly includes argillaceous dolomite, and the main parameters of structural planes have been given above. After inputting parameters in the software, the key blocks formed by various structural planes and their outcrop locations are shown in Fig. 6.

Safety factors and ensemble characteristics of various key blocks are listed in Table 3.

Table 3. Safety factors and geometrical characteristics of key blocks formed in zone Ⅱ

Structural planes forming key blocks	Key blocks	Locations of key blocks	Safety factors	Block volumes (m^3)	Block weights (t)
1, 2, 3	1	Lower right part of chamber wall	29.567	0.054	0.143
	2	Bottom of chamber	Stable	0.005	0.012
	3	Upper right part of chamber wall	4.633	0.057	0.155
	4	Upper left part of chamber wall	10.190	0.216	0.584
	5	Top of chamber	0.000	0.0001	0.001
1, 2, 4	6	Upper left part of chamber wall	3.629	0.149	0.402
	7	Bottom of chamber	Stable	0.111	0.299
	8	Lower right part of chamber wall	34.750	0.029	0.077
	9	Upper right part of chamber wall	4.109	0.054	0.145
	10	Top of chamber	0.000	0.001	0.003
1, 3, 4	11	Lower right part of chamber wall	342.258	0.005	0.014
	12	Bottom of chamber	Stable	0.003	0.009
	13	Upper right part of chamber wall	21.214	0.107	0.288
	14	Upper left part of chamber wall	11.896	0.029	0.077
	15	Top of chamber	0.000	0.0001	0.0001
2, 3, 4	16	Bottom of chamber	Stable	3.438	9.281
	17	Lower right part of chamber wall	89.386	0.003	0.007
	18	Top of chamber	5.505	2.009	5.424
	19	Lower left part of chamber wall	48.032	0.002	0.006

According to Fig. 6 and Table 3, the stability of key blocks is analyzed as follows:

(1) Key blocks 16 and 18 formed by structural planes 2, 3, and 4 have large volumes and weights, and therefore pose a certain threat in principle. Considering that key block 16 is located at the bottom, it is regarded stable. The safety factor of key block 18 is 5.505, which means that it is relatively stable, while some protective measures are suggested to be taken during mining due to its location at the top.

(2) The safety factors of key blocks 5, 10, and 15 are all zero and these key blocks are all located at the top, which theoretically indicates that these key blocks have certain influences on surrounding rock stability of the chamber. However, because of the small volume and weight, these key blocks are considered to have small failure affected zones and regarded stable.

(3) Except for the above key blocks, other key blocks are characterized by large safety factors, while small volumes and weights, so they are all relatively stable. Considering this, the surrounding rocks in the zone are deemed to have high stability.

Stability analysis of surrounding rocks in zones Ⅲ and Ⅳ

The zone can be divided into two sections according to lithology due to changes in the strike of the chamber axis, namely, lithology along survey line D and that along survey line A. Rocks in the zone mainly include limestone. Because of the basically similar simulation input of the software and the length limitation, figures of simulated outcrop locations of key blocks with lithology in the zone are not given. The outcrop locations, safety factors, and geometrical characteristics of key blocks formed by structural planes along survey lines D and A are only provided below.

Key blocks formed by structural planes along survey line D in zone Ⅲ and their parameters are listed in Table 4.

Table 4. Key blocks formed by structural planes along survey line D in zone Ⅲ and their parameters

Structural planes forming key blocks	Key blocks	Locations of key blocks	Safety factors	Block volume (m^3)	Block weight (t)
1, 2, 3	1	Lower right part of chamber	89.910	0.001	0．002
	2	Bottom of chamber	Stable	0.343	0.925
	3	Upper right part of chamber	2.175	0.195	0.526
	4	Upper left part of chamber	17.614	0.016	0.043
	5	Top of chamber	0.000	0.0001	0.001
1, 2, 4	6	Lower left part of chamber	Stable	0.056	0.151
	7	Upper left part of chamber	4.212	0.002	0.007
	8	Upper right part of chamber	1.473	0.604	1.631
	9	Top of chamber	0	0.001	0.004
1, 3, 4	10	Lower right part of chamber	Stable	0.430	1.162
	11	Upper left part of chamber	4.390	1.623	4.381
	12	Top of chamber-1	0.000	0.0001	0.0001
	13	Top of chamber-2	11.483	0.001	0.002
2, 3, 4	14	Bottom of chamber	Stable	1.754	4.735
	15	Lower right part of chamber	43.190	0.001	0.002
	16	Upper left part of chamber	32.032	0.0001	0.0001
	17	Top of chamber	2.454	0.775	2.093
	18	Lower left part of chamber	69.620	0.001	0.003

Based on Table 4, stability of key blocks is analyzed as follows:

(1) Because key blocks 14 and 17 formed by structural planes 2, 3, and 4, as well as key block 8 formed by structural planes 1, 2, and 4 have large volumes and weights, they pose certain threats in principle. Because key block 14 is located at the bottom of the chamber, it is regarded to have relatively high stability. The safety factor of key block 17 is 2.454, so it is relatively stable, while some protective measures should also be taken during mining due to its location at the top. Key block 8 is situated on the right-side wall and has a safety factor lower than 1.5, so it should be paid attention to during excavation.

(2) Key blocks 5, 9, and 12 all have safety factors of zero and they are located at the top. Theoretically, these key blocks exert certain influences on surrounding rock stability of the chamber, while they are considered to have small failure affected zones and regarded stable because of their small volumes and weights.

(3) Except for the above key blocks, other key blocks all have large safety factors while small volumes and weights, which are therefore considered stable. Surrounding rocks in the zone are considered to have high stability.

Key blocks formed by structural planes along survey line A in zone Ⅳ and their parameters are displayed in Table 5.

Table 5. Key blocks formed by structural planes along survey line A in zone Ⅳ and their parameters

Structural planes forming key blocks	Key blocks	Locations of key blocks	Safety factors	Block volume (m^3)	Block weight (t)
1, 2, 3	1	Lower right part of chamber wall	211.578	0.0001	0.001
	2	Bottom of chamber	Stable	0.210	0.566
	3	Upper right part of chamber wall	2.288	0.230	0.622
	4	Upper left part of chamber wall	20.393	0.019	0.051
	5	Top of chamber	0.000	0.001	0.002
1, 2, 4	6	Lower left part of chamber wall	58.544	0.007	0.020
	7	Upper left part of chamber wall	14.047	0.010	0.028
	8	Upper right part of chamber	2.260	0.243	0.656
	9	Top of chamber	Stable	0.152	0.411
	10	Bottom of chamber	0.000	0.004	0.012
1, 3, 4	11	Lower left part of chamber wall	46.415	0.046	0.123
	12	Upper left part of chamber wall	5.262	0.018	0.047
	13	Upper right part of chamber wall	2.985	0.392	1.059
	14	Bottom of chamber	Stable	0.058	0.157
2, 3, 4	15	Bottom of chamber	Stable	8.102	21.876
	16	Lower right part of chamber wall	84.429	0.0001	0.001
	17	Top of chamber	1.376	5.531	14.935
	18	Lower left part of chamber wall	174.358	0.0001	0.001

Based on Table 5, stability of key blocks is analyzed as follows:

(1) Key block 17 formed by structural planes 2, 3, and 4 is characterized by the large volume and weight, and poses a certain threat due to its location at the top of the chamber and a safety factor lower than 1.5. Therefore, some protective measures should be taken during excavation.

(2) The safety factors of key blocks 5 and 10 are both zero. Key block 5 is located at the top of the chamber, so it theoretically exerts certain influence on the surrounding rock stability of the chamber. Whereas, because the key block has small volume and weight, it is regarded to have a small failure affected zone and considered stable. In comparison, key block 10 is situated at the bottom and has small volume and weight, so it is regarded stable.

(3) Aside from the above key blocks, other key blocks all have large safety factors while small volumes and weights, so they are all relatively stable. Surrounding rocks in the zone are considered to have high stability.

5. Conclusions

This paper optimizes block theory based on an improved vector method and utilizes the Unwedge computer program to conduct visual simulations of its applications. This enhances the convenience of applying block theory. To verify the accuracy of the research findings, the Jinping II Hydropower Station's underground cavern is selected as an engineering case for analysis and validation, confirming the feasibility of the research methods proposed in this paper and providing practical and reproducible guidance for actual construction. The conclusions are as follows:

(1) The improved vector method can quickly identify the stability of surrounding rock in different study areas, providing an effective reference for the actual excavation of underground caverns. Based on the theoretical coefficients of surrounding rock stability in underground caverns, the stability patterns of the surrounding rock can be intuitively obtained through visual simulations using the Unwedge computer program and can be mutually verified.

(2) In the I-IV sections, special attention should be paid during excavation when the stability coefficient of key blocks is less than 1.5. Some key blocks have a safety coefficient of zero and are located at the top of the cavern. In theory, these key blocks have a certain impact on the stability of the surrounding rock of the cavern. However, due to the small volume and weight of these key blocks, they can be considered stable.

(3) By comparing the results of the improved block theory and computer program calculations with the actual construction and excavation process of the underground cavern, it is found that they are essentially consistent. This indicates that the innovative method proposed in this paper can provide theoretical support and a feasible basis for the excavation of deeply buried underground caverns.

(4) The results obtained from the improved block theory and the Unwedge computer program provide valuable insights that significantly aid the subsequent stages of structural design for deeply buried underground caverns. By accurately assessing the stability of surrounding rock and identifying critical blocks, engineers can make informed decisions regarding the design of support systems, such as the placement and orientation of rock bolts, shotcrete thickness, and the overall layout of reinforcement. The safety factors and stability patterns derived from these analyses offer a quantitative basis for selecting appropriate support measures, ensuring that the structural design is both safe and cost-effective. Furthermore, the identification of potential failure zones allows for preemptive measures to be implemented during the construction phase, thereby reducing the risk of unforeseen collapses or deformations. In essence, these analyses bridge the gap between geological assessment and practical structural design, contributing to the robustness and reliability of underground engineering projects.

Conflicts of interest

The authors declare that there are no conflicts of interest regarding the publication of this paper.

Data Availability

The data that appeared in this paper will be available upon reasonable request.

References

Abdallah, A. M., Zaki, N. G., El Kerdawy, A. M., Mahmoud, W. H., & Mohamed, G. G. (2023). Coordination behavior of cocaine toward d-block metal ions: synthesis, spectral analysis, density functional theory (DFT) studies, and chemotherapeutic activity. Journal of Molecular Structure, 1293, 136301. https://doi.org/10.1016/j.molstruc.2023.136301

Fu, X., Du, W., Sheng, Q., Chen, J., Fang, Q., & Zhou, Y. (2021). Extensions of the dynamic Newmark method for seismic stability analysis of rock block. International Journal for Numerical and Analytical Methods in Geomechanics, 45(10), 1477-1499. https://doi.org/10.1002/nag.3210

Haryono, I. S., & Purwodihardjo, A. (2021). Discrete fracture network approach in ground support design optimisation for large span cavern in jointed rock mass. In ARMA US Rock Mechanics/Geomechanics Symposium:1180.

He, P., Wang, G., Xu, F., & Sun, S. Q. (2021). GPR-MCS model of reliability analysis of key blocks and its engineering application. International Journal for Numerical and Analytical Methods in Geomechanics, 45(12), 1739-1755. https://doi.org/10.1002/nag.3222

Hosseini, T. V. (2016). Analysis of support pressure for stabilization of rock blocks in the Zaker tunnel. Journal of Structural Engineering and Geo-Techniques, 6(2), 9-20.

Hustrulid, W., & Johnson, G. A. (Eds.). (2020). Rock Mechanics Contributions and Challenges: Proceedings of the 31st US Symposium on Rock Mechanics. CRC Press. https://doi.org/10.1201/9781003078944

Janiszewski, M., Pontow, S., & Rinne, M. (2021). Industry survey on the current state of stope design methods in the underground mining sector. Energies, 15(1), 240. https://doi.org/10.3390/en15010240

Khodr, S., Tonioni, P. L., Lignier, P., Lambrughi, A., Diederichs, M., Ching, I., & Lazzarin, F. (2023). Design criteria for caverns under high stress rock conditions for Snowy 2.0 Power Station Complex. In Expanding Underground-Knowledge and Passion to Make a Positive Impact on the World: 2013-2020. https://doi.org/10.1201/9781003348030-242

Lemos, C. C. D. S., Dias, L. O. F., Barbosa, P. S. D. A., Marques, E. A. G., Ferraz, R. L., & Nalon, G. H. (2024). Digital tools used on the teaching-learning process in geotechnical engineering. Soils and Rocks, 47(2), e2024004923. https://doi.org/10.28927/sr.2024.004923

Lenjani, M. Z., & Nikjo, A. (2021). Roof Tunnel Stability by Wedge Analysis. Journal of Engineering Geology, 14, 163. https://doi.org/10.52547/jeg.14.5.163

Li, W. X., Xue, Z. C., Liu, L. M., Zhang, S., Zhang, F. Y., Li, W. T., & Zhang, C. A. (2024). Failure Mechanism and Active Support of Large-Span Tunnel with Unstable Rock Blocks: A Case Study. Geotechnical and Geological Engineering, 42(7), 5907-5925. https://doi.org/10.1007/s10706-024-02870-w

Lodge, T. P., Seitzinger, C. L., Seeger, S. C., Yang, S., Gupta, S., & Dorfman, K. D. (2022). Dynamics and equilibration mechanisms in block copolymer particles. ACS polymers Au, 2(6), 397-416. https://doi.org/10.1021/acspolymersau.2c00033

Loss, R. (2021). Open future, supervaluationism and the growing-block theory: a stage-theoretical account. Synthese, 199(5), 14249-14266. https://doi.org/10.1007/s11229-021-03419-7

Mahdevari, S., Moarefvand, P., & Mohammadzamani, D. (2020). Considering the effect of block-to-matrix strength ratio on geomechanical parameters of bimrocks. Geotechnical and Geological Engineering, 38, 4501-4520. https://doi.org/10.1007/s10706-020-01304-7

Paraskevopoulou, C., & Boutsis, G. (2020). Cost overruns in tunnelling projects: Investigating the impact of geological and geotechnical uncertainty using case studies. Infrastructures, 5(9), 73. https://doi.org/10.3390/infrastructures5090073

Potvin, Y., Hadjigeorgiou, J., & Wesseloo, J. (2019). Towards optimising ground support systems in underground mines. In Ground Support 2019: Proceedings of the Ninth International Symposium on Ground Support in Mining and Underground Construction:493-502. https://doi.org/10.36487/acg_rep/1925_35_potvin

Qiang, Y., & Li, W. (2021). Accelerated method of self-consistent field theory for the study of gaussian ring-type block copolymers. Macromolecules, 54(19), 9071-9078. https://doi.org/10.1021/acs.macromol.1c01683

Sarkar, T., Sarkar, D., & Mondal, P. (2021). Road network accessibility analysis using graph theory and GIS technology: a study of the villages of English Bazar Block, India. Spatial Information Research, 29(3), 405-415. https://doi.org/10.1007/s41324-020-00360-8

Sengani, F., & Mulenga, F. (2022). A review on the application of particle finite element methods (PFEM) to cases of landslides. International Journal of Geotechnical Engineering, 16(3), 367-381. https://doi.org/10.1080/19386362.2020.1814027

Shrestha, N. (2020). Evaluation on stability condition along the headrace tunnel of Kulekhani-III Hydroelectric Project.

Wang, F., Zhang, H., & Li, D. (2020). Study of Landslide Prevention Schemes Options Using Probability Dom-inance Decision-Making Model. Electronic Journal of Structural Engineering, 20, 13-21. https://doi.org/10.56748/ejse.20241

Zerradi, Y., Lahmili, A., & Souissi, M. (2020). Stability of a rock mass using the key block theory: a case study. In E3S Web of Conferences 150:03024. https://doi.org/10.1051/e3sconf/202015003024

Zhang, M., Wang, T., Wang, X., Wu, W., & Guo, J. (2023). Analysis on the laying method and thermal insulation effect of tunnel insulation layer in high-altitude cold regions. Electronic Journal of Structural Engineering, 23(4), 66-74. https://doi.org/10.56748/ejse.23376

Disclaimer